

Conductivity in a disordered one-dimensional system induced by electron-phonon interaction

A. A. Gogolin, V. I. Mel'nikov, and É. I. Rashba

L. D. Landau Institute of Theoretical Physics, USSR Academy of Sciences

(Submitted February 17, 1975)

Zh. Eksp. Teor. Fiz. 69, 327-349 (July 1975)

An asymptotically exact solution for the electric conductivity of a one-dimensional electron gas interacting with randomly distributed impurities and phonons is obtained. The electron states which are completely localized in a one-dimensional disordered system become nonstationary if the electron-phonon interaction is taken into account. Consequently, a non-vanishing low-frequency electric conductivity arises in the system and is proportional to the interaction in the case of weak electron-phonon interaction. The electric conductivity of such a system is calculated and the carrier diffusion in it is investigated assuming that the impurity potential is sufficiently weak (namely, the localization length ζ_l^- considerably exceeds the interimpurity distance). The diffusion coefficient values are consistent with the idea of electron hops that occur over distances of the order of ζ_l^- and at a period of the order of the phonon relaxation time τ_{ph} . Phonon scattering involving a small momentum transfer, and scattering involving a momentum transfer $\sim 2p_F$, contribute to the process. At low temperatures the first type is predominant, as distinct from the usual phonon resistance mechanism, in which the second type is always predominant. In passim, the asymptotic density correlator $|x|^{-3/2} \exp(-|x|/4\zeta_l^-)$, which determines the nature of localization is calculated for an electron in an impurity field at large distances and times.

PACS numbers: 71.85.Ce, 72.90.+y

1. INTRODUCTION

Interest in disordered one-dimensional systems, which was initially connected mainly with the possibility of obtaining a number of exact results for these systems,^[1] has subsequently increased in connection with experimental investigations of certain systems whose electronic spectra are close to one-dimensional (see, e.g.,^[2]). A very important result is that of Mott and Twose^[3], according to which all states in a disordered one-dimensional system are localized; this result was subsequently proved more rigorously.^[4,5] This distinguishes one-dimensional systems qualitatively from three-dimensional ones, where the localization takes place only in definite sections of the spectrum.^[6-9]

In a system with localized states one should expect the absence of static conductivity. This was proved directly only recently.^[10,11] When account is taken of the electron-phonon interaction, the situation changes significantly, since jumps between individual localized states become possible and are accompanied by the phonon emission or absorption. Violation of the localization leads to a finite conductivity of a diffusion type. In the case of a weak electron-phonon interaction the conductivity is proportional to this interaction. This mechanism is close to that considered by Mott^[12] in connection with the theory of low-temperature hopping conduction in three-dimensional systems, where it leads to a variation like $\exp\{-(T_0/T)^{1/4}\}$.

We construct in this paper a theory of low-frequency conductivity in a one-dimensional system. It is assumed that the scattering by the impurities is weak in the sense that the localization length greatly exceeds the interimpurity distance. In this limit, all the results are asymptotically accurate. The phonons are assumed to be three-dimensional; the interelectron interaction is disregarded.

We follow the method proposed by Berezinskii^[11] but in conjunction with a new variant of the Keldysh diagram technique^[13] for kinetic phenomena. The method yields

results close to those obtained by the Eliashberg technique.^[14]

2. DETERMINATION OF THE MAIN QUANTITIES

We consider a one-dimensional system of electrons that do not interact with one another and have a dispersion law $\epsilon(p)$, are situated in a random potential $V(x)$, and interact with phonons that are assumed to be three-dimensional.

The Hamiltonian of the interaction with the phonon is written in the form

$$H_{e-ph} = \int \psi^+(x) \psi(x) \varphi(x, y, z) \delta(y) \delta(z) dx dy dz, \quad (1)$$

where $\psi(x)$ and $\psi^+(x)$ are the electron operators, and $\varphi(x, y, z)$ are the phonon operators.

We shall calculate below the correlation functions of the current and density operators. It is convenient to introduce for these operators a common symbol $j^a(x)$ ($a = 0; 1$):

$$j^0(x) = \psi^+(x) \psi(x), \quad j^1(x) = 1/2 (\hat{v}(x') - \hat{v}(x)) \psi^+(x) \psi(x') |_{x'=x}, \quad (2)$$

where $\hat{v}(x)$ is the velocity operator:

The correlation functions $\mathcal{R}^a(\omega, k)$ are defined in the usual manner in terms of the exact Heisenberg operators

$$\mathcal{R}^a(\omega, k) = \int_{-\infty}^{\infty} d(x-x') \int_0^{\infty} d(t-t') \exp[i\omega(t-t') - ik(x-x')] \times \langle \text{Sp } \rho \tilde{j}^a(t, x) \tilde{j}^a(t', x') \rangle. \quad (3)$$

Here ρ is the equilibrium density matrix, and the angle brackets denote averaging over the realizations of the random potential. The contribution to the correlator from the unconnected diagrams, which does not depend on the coordinates and the time, is omitted throughout. The current-current correlator determines directly, according to the Kubo formula, the conductivity of the system

$$\sigma(\omega, k) = e^2 T^{-1} \mathcal{F}^a(\omega, k), \quad (4)$$

where T is the temperature. Formula (4) is suitable so long as $\omega \ll T$, a condition that will henceforth be assumed satisfied.

Calculation of the density-density correlator makes it possible to follow the manner in which a quasilocal electronic state becomes smeared out under the influence of the interaction with the phonons. We shall determine in passing the diffusion coefficient.

The correlators will be calculated by the Keldysh matrix technique.^[13] Accordingly, we represent the electron and phonon Green's functions in the form of the matrices $\mathcal{G}_{\alpha\alpha'}$ and $\mathcal{D}_{\alpha\alpha'}$. When ordered in time, all the operators with index $\alpha = 2$ in the Green's functions are to the left of (i.e., "later" than) the operators with $\alpha = 1$. The operators with $\alpha = 1$ are arranged relative to one another in the usual chronological order, while the operators with $\alpha = 2$ are arranged in inverse order.

In the absence of interaction, the electron Green's function takes in the coordinate-energy representation the form

$$\mathcal{G}_0(x|x') = G_0^- A^- \cdot I + G_0^+ I \cdot A^+. \quad (5)$$

Here G_0^+ and G_0^- are the retarded and advanced quantum-mechanical Green's functions

$$G_0^\pm(x|x') = \int \frac{dp}{2\pi} \frac{e^{ip(x-x')}}{\epsilon - \epsilon(p) \pm i0} = \mp \frac{i}{v(\epsilon)} \exp(\pm ip(\epsilon)|x-x'|), \quad (6)$$

where $\epsilon(p)$ is the electron dispersion law, $\rho(\epsilon)$ is the positive root of the equation $\epsilon = \epsilon(p)$, and $v(\epsilon) = d\epsilon/dp$ is the electron velocity. The dot in (5) denotes a dyadic product of the vectors

$$A^- = \begin{pmatrix} n \\ n-1 \end{pmatrix}, \quad A^+ = \begin{pmatrix} 1-n \\ -n \end{pmatrix}, \quad I = \begin{pmatrix} 1 \\ 1 \end{pmatrix}, \quad (7)$$

which is defined in the usual manner: $(A \cdot B)_{ij} = A_i B_j$. In (7), $n(\epsilon)$ is the Fermi distribution function. The phonon Green's function is given by

$$D(\Omega, q) = |c_q|^2 \left\{ \frac{1}{\Omega - \omega_q + i0} \begin{pmatrix} N_q + 1 & N_q \\ N_q + 1 & N_q \end{pmatrix} + \frac{1}{\Omega + \omega_q + i0} \begin{pmatrix} N_q & N_q + 1 \\ N_q & N_q + 1 \end{pmatrix} - \frac{1}{\Omega + \omega_q - i0} \begin{pmatrix} N_q + 1 & N_q + 1 \\ N_q & N_q \end{pmatrix} - \frac{1}{\Omega - \omega_q - i0} \begin{pmatrix} N_q & N_q \\ N_q + 1 & N_q + 1 \end{pmatrix} \right\}, \quad (8)$$

where c_q is the matrix element of the electron-phonon interaction and N_q is the Planck distribution function.

In such a technique, we can calculate directly the matrix correlators

$$\mathcal{F}_{\alpha\alpha'}(\omega, k) = \int_{-\infty}^{\infty} d(x-x') \int_{-\infty}^{\infty} d(t-t') e^{i\omega t - i t' - ik(x-x')} \times \langle \text{Sp} \rho T \{ \tilde{j}_{\alpha\alpha'}(t, x) \tilde{j}_{\alpha'\alpha'}(t', x') \} \rangle, \quad (9)$$

the time ordering in (9) being effected with allowance for the values of the times (t, t') as well as of the matrix indices (α, α'). The correlators $\mathcal{Z}^a(\omega, k)$ are expressed in terms of $\mathcal{F}^a(\omega, k)$ in the following manner:

$$\mathcal{Z}^a(\omega, k) = \frac{1}{2\pi i} \int_{-\infty}^{\infty} \mathcal{F}_{21}(\omega', k) \times \frac{d\omega'}{\omega' - \omega - i0}. \quad (10)$$

The quantities \mathcal{F}^a correspond to diagrams in the form of the electron loop shown in Fig. 1, in the two vertices of which are located the operators j^a (the exclusion of more complicated diagrams is discussed in the Appendix). On the diagrams, the electron Green's functions are shown by solid lines (single for G_0^+ and double for G_0^-), the phonon functions by dashed lines, and the correlators of the random potential by wavy lines.

3. DIAGRAM TECHNIQUE FOR AN ELECTRON IN THE FIELD OF IMPURITIES

We start with a model of randomly distributed centers, and consider the scattering of the electrons by these centers in the Born approximation. The potential of an individual impurity is assumed to decrease rapidly, i.e., its width d is much less than the average distance c^{-1} between the impurities (c is the impurity concentration).

In the Born approximation, the mean free path l_i is much larger than the distance between impurities, so that $d \ll c^{-1} \ll l_i$. Under these conditions, the impurity-potential correlator

$$U(x-x') = \langle V(x)V(x') \rangle \quad (11)$$

has a width on the order of d ; it reflects the form factor of the impurity potential. The electron wavelength λ is also assumed small in comparison with l_i ($\lambda \ll l_i$); the ratio of λ to d can be arbitrary.

We show first how to change over from diagrams containing the matrix functions \mathcal{G}_0 to diagrams containing G_0^\pm . Each impurity vertex corresponds to a matrix $\hat{V} = V\sigma_z$. The dyadic structure of the function \mathcal{G}_0 (see (5)) makes it possible to assign the individual vectors I and A^- (or A^+ and I) to vertices in which an electron line terminates and begins, respectively. Carrying out matrix multiplication in the impurity vertices, we obtain

$$I\sigma_z I = A^+ \sigma_z A^- = 0, \quad I\sigma_z A^- = A^+ \sigma_z I = 1. \quad (12)$$

It follows from these relations that any impurity vertex to which a single and double line converge is annihilated. Vertices to which lines of one type converge enter in the diagrams with a factor V . Therefore each of the electron lines joining the points x and x' consists exclusively of single or of double lines, which yields as a sum the resolvents $G^\pm = (\epsilon - H_0 - V \pm i0)^{-1}$ where $H_0 = \epsilon(-i\nabla_x)$. Thus, the summation over the matrix indices leads to a simple technique for the internal vertices; its application to the external vertices is perfectly analogous. In final analysis, the calculation of the mean values of the quantities $\mathcal{G}_{\alpha\alpha'} \mathcal{G}_{\alpha'\alpha}$ in $\mathcal{F}_{\alpha\alpha'}$ (cf. Fig. 1) reduces to a calculation of the mean values of $G_i G_{i'}$ ($i, i' = \pm$). For the latter mean values, a convenient technique, as applied to δ -function correlators $U(x-x')$, was developed by Berezinskiĭ.^[11] This technique is based on a consideration of diagrams that are ordered in accordance with the coordinate. In each integration interval it is possible to replace $|x-x'|$ by $\pm(x-x')$ in the arguments of the exponentials in the

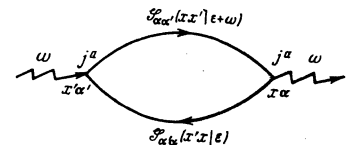


FIG. 1. Electron loop corresponding to the correlator $\mathcal{F}_{\alpha\alpha'}(xx'|\omega)$.

Green's functions G_0^+ and G_0^- (6), to break up the Green's functions into the factors

$$(\mp i/v(\epsilon))^{1/2} e^{\pm i p(\epsilon)x} \text{ and } (\mp i/v(\epsilon))^{-1/2} e^{\mp i p(\epsilon)x'} \quad (13)$$

and to include these factors in the corresponding impurity vertices. It can then be verified that in the Born approximation only two types of factors appear in the essential diagrams (see below), corresponding to different impurity lines:

$$\pm \frac{1}{v^2(\epsilon)} U(x-x') \text{ и } \pm \frac{1}{v^2(\epsilon)} U(x-x') e^{\pm 2i p(\epsilon)(x-x')}, \quad (14)$$

which correspond respectively, for example, to diagrams of type a, b and c, d in Fig. 2.

To use the convenient technique developed for δ -function correlators (which correspond graphically to vertical impurity lines), it is expedient when integrating over the coordinates of the impurity vertices to carry out the integration first with respect to the "internal" variables, i.e., with respect to the differences $x - x'$. These integrations for different impurity lines can be carried out independently if one excludes the more complicated vertices, for example such as Fig. 2e. In these diagrams, the integrations corresponding to two different impurity lines are carried out over one and the same region having a width on the order of d . Since the effective integration region in the diagrams is determined by the damping of the Green's functions and is therefore of order l_1 , the contribution of the diagrams of the type of Fig. 2e is small in terms of the parameter d/l_1 .

All the contributions corresponding to the impurity lines in spatially ordered diagrams are expressed in terms of the integrals

$$\frac{1}{l_1^+(\epsilon)} = \frac{2}{v^2(\epsilon)} \int_0^\infty U(x) dx, \quad \frac{1}{l_1^-(\epsilon)} \pm \frac{i}{l_1^0(\epsilon)} = \frac{2}{v^2(\epsilon)} \int_0^\infty U(x) e^{\pm 2i p(\epsilon)x} dx. \quad (15)$$

The lines of the type of Fig. 2a correspond to a contribution $(-l_1^+)^{-1}$, and the lines of the type of Fig. 2c correspond to $(-l_1^-)^{-1}$; diagrams b and d merge into a single one corresponding to the contribution $(-2l_1^0)^{-1} + (-2l_1^-)^{-1} + i(-2l_1^0)^{-1}$. We see thus that the impurity lines can be drawn in the diagrams vertically (just as for δ -function correlators), but they must be set in correspondence with different contributions for diagrams with rotation (Fig. 2c) and without rotation (Fig. 2a) of the electron lines, and also for the self-energy inserts (Figs. 2b and 2d). The quantities l_1^+ and l_1^- have the meaning of the mean free path with respect to forward and backward scattering.

It remains to select the essential diagrams, using the condition $\lambda \ll l_1$, which is equivalent to $\epsilon \gg \tau_1^{-1} = l_1^-/v$. This selection can be carried out at an external frequency $\omega \ll \epsilon$; the parameter $\omega\tau_1$ can then be arbitrary. The selection is based on neglecting the contri-

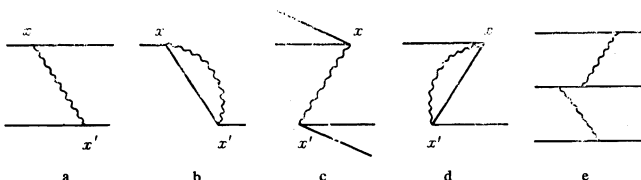


FIG. 2

butions of the diagrams containing factors of the type $e^{2ip(\epsilon)x}$, which oscillate rapidly over the mean free path l_1 in comparison with the diagrams that contain only smooth factors of the type $e^{i\omega x/v}$. Since the structure of our diagrams is now practically the same as in Berezinskii's paper, we can use his results directly.

Figure 3 shows all the types of the impurity lines that enter in the essential diagrams, and indicates the contributions corresponding to them. These contributions were calculated in the lowest order in ω/ϵ , so that the term linear in ω is retained only in the argument of the exponential. With respect to the same parameter ω/ϵ it is necessary to retain in the loop of Fig. 1 only the products $G^+(\epsilon + \omega)G^-(\epsilon)$ and $G^-(\epsilon + \omega)G^+(\epsilon)$. Since the second product vanishes in the integration in (10), we shall discard it throughout; this corresponds to a transition from the correlators \mathcal{F} to the corresponding quantities \mathcal{X} (when used in the impurity problem, we shall designate them by X).

We put $x > x'$. Then each diagram can be subdivided into three parts: right (to the right of x), central (between x and x'), and left (to the left of x'). Examining the "passages" of the individual impurity lines through the point x as the latter is displaced, we can obtain the following equations for the right and central parts $-R_m(x)$ and $Z_{m'm}(x', x)$:

$$-\frac{dR_m}{dx} = \frac{1}{l_1^-} \{m^2 R_{m-1} e^{2i\omega x/v} + m^2 R_{m+1} e^{-2i\omega x/v} - 2m^2 R_m\}, \quad (16)$$

$$\frac{dZ_{m'm}}{dx} = \frac{i\omega}{v} Z_{m'm} + \frac{1}{l_1^-} \{m^2 Z_{m'm-1} e^{-2i\omega x/v} + (m+1)^2 Z_{m'm+1} e^{-2i\omega x/v} - (m^2 + (m+1)^2) Z_{m'm}\}. \quad (17)$$

The index m shows that $2m$ single and $2m$ double lines enter in the point x in the right part $R_m(x)$; the number of these lines is the same, since it is changed only by the vertices of type e and f of Fig. 3. In the central part $Z_{m'm}(x', x)$, $2m' + 1$ lines of each type enter the point x' , while $(2m + 1)$ lines enter the point x . The coefficients of $R_{m \mp 1}$ are determined by the number of manners in which the lines e and f can be connected (Fig. 3). The coefficient of R_m in (16) is made up of the contributions of the impurity lines $a(a')$, $b(b')$, $c(c')$ and d:

$$-2m(1/2l_1^+ + 1/2l_1^- + i/2l_1^0) - 2m(1/2l_1^+ + 1/2l_1^- - i/2l_1^0) - 2m(2m-1)/l_1^+ - 2m(m-1)/l_1^- + (2m)^2/l_1^+ = -2m^2/l_1^-, \quad (18)$$

We see that the final equations contain only the mean free path with respect to scattering with reversal of the momentum. This is quite natural, since only elastic

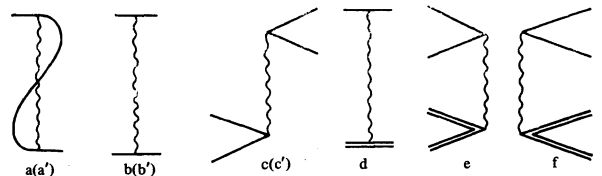


FIG. 3. Types of impurity lines entering in the essential diagrams. A single line corresponds to G_0^+ and a double line to G_0^- . The wavy line corresponds to the impurity correlator. Diagrams a', b', and c' differ from a, b, and c in that the single lines are replaced by double lines. The lines correspond to the following factors: a) $-1/2l_1^- - 1/2l_1^- - i/2l_1^0$; a') $-1/2l_1^- - 1/2l_1^+ + i/2l_1^0$; b) $-1/l_1^+$; c, c') $-1/l_1^-$; d) $1/l_1^+$; e) $e^{2i\omega y(\epsilon)/l_1^-}$; f) $e^{-2i\omega y(\epsilon)/l_1^-}$.

scattering of this kind is meaningful in a one-dimensional system.

The correlators (10) for the electrons in the field of the impurities, with allowance for the matrix structure of the Green's functions (5), are expressed in terms of the mean values $\langle n(1-n)G^-(\epsilon)G^+(\epsilon+\omega) \rangle$ and are equal to

$$X^0(\omega, k) = 4 \int \frac{d\epsilon}{2\pi} n(\epsilon) (1-n(\epsilon)) \frac{1}{v(\epsilon)} X^0(\epsilon, \omega, k), \quad (19)$$

$$X^0(\epsilon, \omega, k) = \frac{2l_i^-}{v(\epsilon)} \left[\frac{v(\epsilon)}{2} \right]^{2a} \sum_{m=0}^{\infty} P_m^a(\omega) \{Q_m^a(\omega, k) + Q_m^a(\omega, -k)\}. \quad (20)$$

The factor $n(1-n)$ in (19) is due to the external vertices. The quantities $P_m^a(\omega)$ and $Q_m^a(\omega, k)$ in these formulas are connected with $R_m(x)$ and $Z_m'(x)$ by the relations

$$R_m(x) = R_m e^{2im\omega x/\epsilon}, \quad P_m^0 = 1/2(R_m + R_{m+1}), \quad P_m^1 = R_m - R_{m+1}, \quad (21)$$

$$Q_m^a(\omega, k) = \frac{1}{l_i^-} \sum_{m'=0}^{\infty} \int_{x'}^{\infty} dx e^{ik(x'-x)} e^{-2i\omega m'x'/v} Z_{m'm}(x', x) e^{2i\omega m x/v} P_{m'}^a. \quad (22)$$

The quantities R_m and Q_m^a are determined by the system of equations

$$ivR_m + m(R_{m+1} + R_{m-1} - 2R_m) = 0, \quad (23)$$

$$iv(m+1/2)Q_m^a + (m+1)^2\{Q_{m+1}^a - Q_m^a\} - m^2\{Q_m^a - Q_{m-1}^a\} - ikQ_m^a + P_m^a = 0. \quad (24)$$

The dimensionless frequency and momentum are equal to

$$\nu = 2l_i^- \omega / v = 2\omega \tau_i, \quad \kappa = kl_i^-. \quad (25)$$

4. CORRELATION FUNCTIONS FOR AN ELECTRON IN THE FIELD OF IMPURITIES

Formulas (19) and (20) for the correlators enables us, first, to solve the problem of electron localization in an impurity field. The character of the localization of the electron states is determined by the behavior of the correlator of the electron density at large distances $|x-x'| \gg l_i^-$ and at large times $|t-t'| \gg \tau_i = l_i^-/v$. These times correspond to low frequencies $\nu \ll 1$. In this limit, the decisive contribution is made by diagrams with large $m \sim \nu^{-1}$, and it is therefore possible, just as in Berezinskiĭ's paper,^[11] to go over from the algebraic systems (23) and (24) to differential equations, and from summation over m to integration. From the equation for R_m it follows that^[11]

$$P^0(\zeta) = 2\zeta^{1/2} K_1(2\zeta^{1/2}), \quad \zeta = -ivm, \quad (26)$$

K_1 is a Bessel function. The equation for $Q^0(\zeta, \kappa)$, with (26) taken into account, is of the form

$$-\zeta Q^0 + \frac{d}{d\zeta} \left(\zeta^2 \frac{dQ^0}{d\zeta} \right) - ikQ^0 + 2\zeta^{1/2} K_1(2\zeta^{1/2}) = 0, \quad (27)$$

and we shall investigate its solutions in detail below. The substitution $z = 2\zeta^{1/2}$ transforms (27) into an inhomogeneous Bessel equation for the function $zQ^0(z)$. A solution of this equation, integrable at zero and decreasing at infinity, is

$$Q^0(z) = \frac{4}{z} \left[I_1(z) \int_0^{\infty} \xi d\xi K_1(\xi) K_1(\xi) + K_1(z) \int_0^z \xi d\xi I_1(\xi) K_1(\xi) \right] \quad (28)$$

$$\lambda = (1+4i\kappa)^{1/2}.$$

Going over in (20) from summation over m to integration with respect to $\xi = -ivm$ and rotating the integration contour from the imaginary axis to the real one, we obtain

$$X^0(\epsilon, \omega, k) = \frac{1}{-i\omega} \int_0^{\infty} d\zeta P^0(\zeta) [Q^0(\zeta, \kappa) + Q^0(\zeta, -\kappa)]. \quad (29)$$

We see from this that the singularity in $\omega = 0$, and therefore the long-term asymptotic behavior of the density correlator is indeed determined by the behavior of $X^0(\epsilon, \omega, k)$ at small ω . From (28) and (29) we obtain an expression for the long-term density correlator

$$X^0(\epsilon, t \rightarrow \infty, x) = p_{\infty}(x) = \frac{1}{l_i^-} \int_{-\infty}^{\infty} \frac{d\kappa}{2\pi} \exp(ixx/l_i^-) [f(\kappa) + f(-\kappa)], \quad (30)$$

where

$$f(\kappa) = 4 \int_0^{\infty} z dz K_1(z) I_1(z) \int_0^{\infty} \xi d\xi K_1(\xi) K_1(\xi). \quad (31)$$

The integral in (30) is an even function of x , so that it suffices to evaluate it at $x > 0$. It is convenient to change the order of integration, first integrating with respect to κ . At any finite value of z the only singularity of the integrand in the upper half-plane is the branch point $\kappa = i/4$. By shifting the contour of integration with respect to κ into the upper half-plane in such a way that it follows the edges of the cut drawn from this point upward along the imaginary axis, and making the substitution $\lambda^2 = 1 + 4i\kappa = -\eta^2$, we obtain

$$\int_{-\infty}^{\infty} d\kappa \exp(ixx/l_i^-) I_1(z) K_1(\xi) = \frac{-i}{\pi} \int_0^{\infty} \eta d\eta \exp\left(\frac{-(\eta^2+1)x}{4l_i^-}\right) \times \sin(\pi i\eta) K_{i\eta}(z) K_{i\eta}(\xi). \quad (32)$$

At $x \gg l_i^0$ the significant values in the integral with respect to η are $\eta \sim (l_i^-/x)^{1/2} \ll 1$, so that $K_{i\eta}$ can be replaced by K_0 and $\sin(\pi i\eta)$ by $\pi i\eta$. As a result we have

$$p_{\infty}(x) \approx \frac{1}{4\pi^{1/2} l_i^-} \left(\frac{\pi^2}{8} \right)^{1/2} \left(\frac{4l_i^-}{|x|} \right)^{1/4} \exp\left(-\frac{|x|}{4l_i^-}\right), \quad |x| \gg l_i^-. \quad (33)$$

The correlator thus decreases at large x , for the most part exponentially with a characteristic length determined by the mean free path (in full accord with Mott's qualitative conclusions^[3]). This decrease is further enhanced by the pre-exponential factor $\sim |x|^{-3/2}$. It is seen from this conclusion that the argument of the exponential is determined fully by the position of the branch point $\kappa = i/4$. The magnitude and the coordinate dependence of the pre-exponential factor are determined by the behavior of the integrand on the edges of the cut. Our result for the asymptotic value of the density correlator differs from that obtained by Berezinskiĭ^[11] who determined the asymptotic form from the behavior of $X^0(\epsilon, \omega, k)$ at small $\kappa \ll 1$ (when comparing with Berezinskiĭ's result it must be taken into account that owing to the difference in the notation our l_i^- in^[11] corresponds to $4l$).

It follows from (33) that localized eigenfunctions exist. However, (29) contains in essence an even stronger statement, that all the eigenfunctions are localized. This statement follows from the fact that (29) breaks up into a product of functions of ω and κ ; the numerator, which depends on κ , is equal to 1 at $\kappa = 0$ and changes over distances on the order of $\kappa \sim 1$ (which do not depend on ω).

The next task is to find the behavior of $X^0(\epsilon, \omega, k)$ at small momenta $\kappa \ll 1$ and low frequencies $\nu \ll 1$. It will be shown below that this behavior determines the diffusion rate in the presence of weak interaction with phonons. In this region of parameters, the expansion of formula (29) for X^0 is of the form

$$X^0(\epsilon, \omega, k) = i(1 - A\kappa^2)/\omega. \quad (34)$$

The expansion in powers of κ is best carried out by differentiating (27) in succession with respect to κ and then putting $\kappa = 0$. This yields a chain of equations similar to (27), with only the free terms different. Solving them in succession, we obtain expressions analogous to (28). Ultimately,

$$Q^{\nu}(\xi, \kappa=0) = -\frac{dP^{\nu}}{d\xi}; \quad \left. \frac{dQ^{\nu}(\xi, \kappa)}{d\xi} \right|_{\kappa=0} = -\frac{i}{2\xi} \left[P^{\nu} \ln \xi + 2CP^{\nu} - \frac{dP^{\nu}}{d\xi} \right],$$

$$\left. \frac{d^2 Q(\xi, \kappa)}{d\xi^2} \right|_{\kappa=0} = -\frac{16}{\xi^3} \left\{ I_1(2\xi^{3/2}) \int_0^{\infty} \frac{d\xi}{\xi^2} K_1(\xi) \left[\left(C + \ln \frac{\xi}{2} \right) \xi K_1(\xi) \right. \right.$$

$$\left. \left. + K_0(\xi) \right] + K_1(2\xi^{3/2}) \int_0^{\infty} \frac{d\xi}{\xi^2} I_1(\xi) \left[\left(C + \ln \frac{\xi}{2} \right) \xi K_1(\xi) + K_0(\xi) \right] \right\}, \quad (35)$$

where C is the Euler constant. Substitution in (29) after integration leads to

$$A = 8 \int_0^{\infty} \frac{dz}{z} K_0(z) \left[\left(C + \ln \frac{z}{2} \right) z K_1(z) + K_0(z) \right]. \quad (36)$$

Calculation of this integral is best carried out by introducing a finite lower integration limit and integrating by parts:

$$A = \lim_{z_0 \rightarrow 0} 8 \left[-\frac{K_0^2(z_0)}{2} \left(C + \ln \frac{z_0}{2} \right) + \frac{3}{2} \int_{z_0}^{\infty} K_0^2(z) \frac{dz}{z} \right]. \quad (37)$$

The resultant indefinite integral can be calculated by using formula (5.55) of [15]. Taking the limit as $z_0 \rightarrow 0$ we obtain $A = 4\zeta(3) \approx 4.81$, where ζ is the Riemann zeta function.¹⁾ As shown by Berezinskiĭ^[11] the same integral (36) determines also the low-frequency correlator ($\nu \ll 1$) for an electron in the field of impurities:

$$X^{\nu}(\epsilon, \omega) = -i\omega A (l_i^{-}(\epsilon))^2. \quad (38)$$

5. DIAGRAM TECHNIQUE FOR AN ELECTRON INTERACTING WITH PHONONS

We now proceed directly to a solution of the main problem of the influence of phonons on the kinetic properties of the electron system.

The scattering of the electron by the phonons is accompanied by a change of energy, and differs qualitatively in this respect from scattering by the impurities. Allowance for the interaction with the phonons leads to the appearance in the diagrams of a new scale of the order of the phonon frequency $\omega_{\mathbf{q}}$. We assume the characteristic phonon frequency $\bar{\omega}$ and the width of the phonon spectrum Δ to be large in comparison with the probabilities of scattering by the impurities and phonons: $\bar{\omega}, \Delta \gg \tau_i^{-1}, \tau_{ph}^{-1}$.

It is convenient first, in analogy with the procedure used in Sec. 3 for impurity lines, to integrate with respect to the "internal" variables in diagrams containing phonon lines. The effective spatial width of the phonon D-function is of the order of $x \sim (\bar{q})^{-1}$, where \bar{q} is the characteristic momentum of the phonons. Therefore the contribution of diagrams in which the integrations for the different phonons fall in one spatial region of width $\sim (\bar{q})^{-1}$ (they are analogous to diagram 2e for impurities) will be small in terms of the parameters $(\bar{q}l_i)^{-1}$ and $(\bar{q}l_{ph})^{-1}$. Neglecting diagrams of this kind, we can integrate with respect to the "internal" variables. Then the phonon line corresponds to a contribution proportional to the integral

$$2 \int_0^{\infty} d(x_1 - x_2) \exp\{i(p(\epsilon) \mp p(\epsilon - \Omega))(x_1 - x_2)\} D(\Omega, x_1 - x_2) = L^{\pm}D + iL_{\pm}^{\circ}D.$$

$$L^{\pm}D = \int \frac{d^3\mathbf{q}}{(2\pi)^3} D(\Omega, \mathbf{q}) \delta(q_x + p(\epsilon) \mp p(\epsilon - \Omega)). \quad (39)$$

The contributions $L^{\pm}D$ and $L^{\circ}D$ correspond respectively to diagrams a and b of Fig. 4, i.e., to scattering without and with rotation of the electron lines.

The phonon lines can now be drawn in the diagrams vertically, and it remains only to carry out the integration with respect to their positions.

The next step is to sum over the matrix index in all the internal vertices. This operation is performed, just as for the impurity vertices, using the dyadic structure of \mathcal{G} (cf. (5)), by referring the individual vectors of the dyad to neighboring vertices. The contributions obtained in this manner for those phonon lines which are of importance to us in what follows (see Fig. 5) are shown below: for diagrams a(a') we have

$$\frac{-1}{v(\epsilon)v(\epsilon - \Omega)} \frac{i}{2} (L^{\pm} \pm iL_{\pm}^{\circ} + L^{\mp} \mp iL_{\mp}^{\circ}) [(1 - n(\epsilon - \Omega))D_{21}(\Omega) + n(\epsilon - \Omega)D_{12}(\Omega)].$$

The upper signs correspond to diagram a' and the lower to a. For diagram b we have

$$\frac{1}{v(\epsilon)v(\epsilon - \Omega)} \exp\left\{i\omega y \left(\frac{1}{v(\epsilon - \Omega)} - \frac{1}{v(\epsilon)} \right)\right\} iL^{\pm} [n(\epsilon)D_{21}(\Omega) + (1 - n(\epsilon))D_{12}(\Omega)].$$

For diagrams c and d we have

$$\frac{1}{v(\epsilon)v(\epsilon - \Omega)} \exp\left\{\pm i\omega y \left(\frac{1}{v(\epsilon - \Omega)} + \frac{1}{v(\epsilon)} \right)\right\} iL^{\mp} [n(\epsilon)D_{21}(\Omega) + (1 - n(\epsilon))D_{12}(\Omega)].$$

The upper and lower signs correspond to diagrams c and d, respectively.

As a result we obtain a technique in which the matrix index is no longer involved and which differ from the usual Feynman technique mainly in that the retarded and advanced functions (single) and double lines) enter in it separately. This technique can be used to consider kinetic phenomena at finite temperatures.

The selection of the essential diagrams is based on taking into account expressions that contain only smooth factors of the type $\exp(i\omega x/v)$, and neglecting the diagrams containing rapidly oscillating factors of

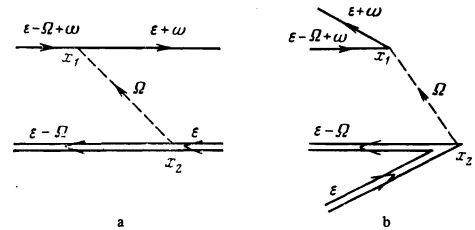


FIG. 4. "Canted" phonon lines.

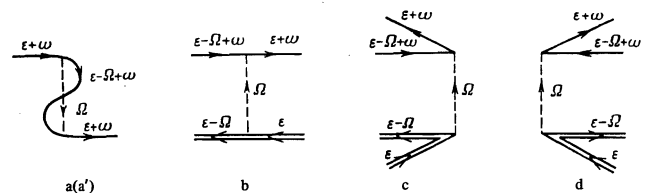


FIG. 5. Types of phonon lines entering in the essential diagrams. The lines a' differ from a in that the single lines are replaced by double ones.

the type $\exp\{i(p(\epsilon) \pm p(\epsilon \pm \omega_Q))y\}$, $\exp\{i(p(\epsilon) \pm p(\epsilon + \omega_Q - \omega_\tau))y\}$, etc. Integrals containing these factors are small in comparison with integrals of the smooth functions with respect to the parameters $(\tau\epsilon)^{-1}$, $(\tau\bar{\omega})^{-1}$, and $(\tau\Delta)^{-1}$. The values of the parameters $\omega\tau_i$ and $\omega\tau_{ph}$ remain arbitrary for the time being.

First to appear, owing to the presence in the diagrams of electron lines corresponding to different energies (that differ by amounts on the order of $\bar{\omega}$ or Δ), are additional restrictions on the impurity lines. It is easily seen that electron lines with different energies can be joined only by impurity lines of the type b(b') and d of Fig. 3. The impurity lines c(c'), e, and f can join only electron lines with equal energies; in other cases the contribution of these diagrams is small in terms of the parameters $(\tau_i\bar{\omega})^{-1}$ and $(\tau_i\Delta)^{-1}$.

Figure 5 shows all the essential phonon diagrams. In connection with the construction of these diagrams we note that, owing to the additional limitations due to the expansion in the parameters $(\tau\bar{\omega})^{-1}$ and $(\tau\Delta)^{-1}$, certain phonon diagrams turn out to be inessential, although the impurity diagrams that are analogous to them are large. On the other hand, the class of competing diagrams is larger, since lines of different types can converge in the phonon vertices (in contrast to the impurity vertices!). Examples of such diagrams, in which single lines are transformed into double lines, are shown in Fig. 6. The first of these diagrams vanishes in the general case. This can be demonstrated by direct calculations, if it is recognized that

$$\int d\Omega G_0^+(\epsilon-\Omega)(D_{11}(\Omega)-D_{21}(\Omega)) = \int d\Omega G_0^-(\epsilon-\Omega)(D_{11}(\Omega)-D_{12}(\Omega)) = 0. \quad (40)$$

The contributions of diagrams b and c of Fig. 6 differ from zero only if the energies of one of the upper and one of the lower electron lines do not coincide. This can be verified by direct calculation using the relation

$$D_{12}(\Omega)(1-n(\epsilon))n(\epsilon-\Omega) = D_{21}(\Omega)(1-n(\epsilon-\Omega))n(\epsilon), \quad (41)$$

which represents the detailed-balancing principle, and using the identity^[13]

$$D_{11}+D_{22}=D_{12}+D_{21}. \quad (42)$$

At $\epsilon \neq \epsilon'$ the contribution of these diagrams differs from zero, since the occupation numbers $n(\epsilon)$ and $n(\epsilon')$ are not cancelled out. The contribution of diagram d of Fig. 6 differs from zero at all times.

Diagrams b-d of Fig. 6 can introduce either the usual oscillatory factors of the type $\exp\{i(p(\epsilon) \pm p(\epsilon \pm \omega_Q))y\}$, or factors of the type

$$\exp\{i(p(\epsilon)-p(\epsilon-\Omega)+p(\epsilon'-\Omega)-p(\epsilon'))y\} \approx \exp\left\{i\frac{\Omega}{v^2}\frac{dv(\epsilon)}{d\epsilon}(\epsilon'-\epsilon)y\right\}; \quad |\Omega|, |\epsilon'-\epsilon| \ll \epsilon. \quad (43)$$

The diagrams containing the former factors are small in the parameter $(\bar{\omega}\tau)^{-1}$. The factors of the latter type

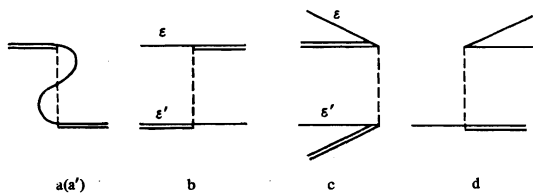


FIG. 6. Phonon vertices in which electron lines of various types converge.

oscillate over distances $\sim \epsilon v/\bar{\omega}^2$ (at $|\epsilon' - \epsilon| \sim \bar{\omega}$) and make a small contribution only if $\bar{\omega}\tau\beta = \bar{\omega}\tau\bar{\omega}/\epsilon \gg 1$. Under quasielasticity conditions $\beta \ll 1$ this criterion is much more stringent than $\bar{\omega}\tau \gg 1$. Nonetheless, whenever we refer to a degenerate electron gas below we shall assume this criterion to be satisfied.

The diagrams containing lines of the type b-d of Fig. 6 are proportional to higher powers of the occupation numbers n and in the case of a nondegenerate electron gas ($n \ll 1$) they can be omitted regardless of the value of the parameter $\bar{\omega}\tau\beta$. The diagrams of Fig. 6 will be omitted throughout from now on.

We proceed now to phonon vertices that have analogs among the impurity vertices. By way of example we point out diagrams a and b of Fig. 7, which are analogous to diagram b of Fig. 3. The phonon line of diagram a of Fig. 7 introduces by itself a rapidly-oscillating factor that leads to the appearance of the small factor $(\bar{\omega}\tau_{ph})^{-1}$.

The situation is much more complicated with the phonon line b of Fig. 7. By itself it does not introduce a rapidly oscillating factor, but it can be included in the diagrams only in the presence of rotating vertices, impurity or phonon. The corresponding impurity lines (e.g., of type e or f of Fig. 3) will always join lines with different energies, and the diagrams will be small in the parameter $(\bar{\omega}\tau_i)^{-1}$. On the other hand if line b of Fig. 7 is included in the diagram with the aid of rotating phonon vertices of the type c or d of Fig. 6, then this entails the appearance of a factor $(\bar{\omega}\tau\beta)^{-1}$. As a net result both diagrams a and b of Fig. 7, as well as certain other diagrams, can be left out.

A typical diagram constructed of phonon lines of Fig. 5 is shown in Fig. 8. It has the same structure as the diagrams that are usually taken into account in the derivation of the kinetic equation. It contains two types

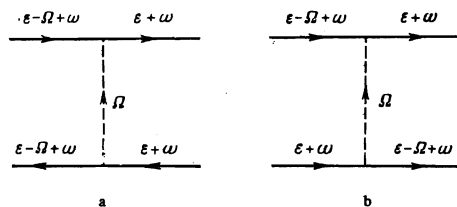


FIG. 7

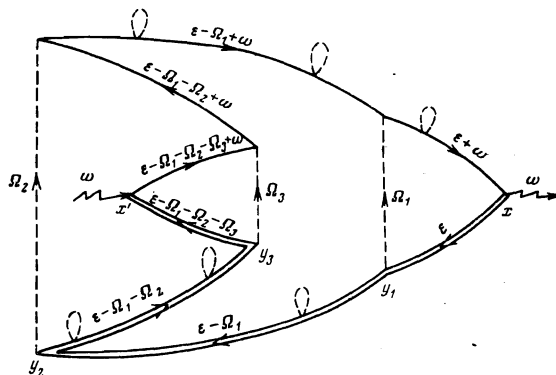


FIG. 8. Typical skeleton diagram for a correlator with allowance for the essential phonon lines. The impurity lines are not shown. The dashed loops correspond to the self-energy diagrams of type a(a') of Fig. 5.

of phonon line. The first, represented by the loops, are self-energy parts of type $a(a')$ of Fig. 5. They correspond to outflow of the particles from the given state. The second, which join the upper and lower electron lines, divide the diagrams into sections within which the energies corresponding to these lines are identical, accurate to a small external frequency ω (they correspond to the inflow of particles). This is a skeleton diagram, since it must be supplemented with all the admissible impurity lines. The structure of the resultant diagrams becomes very much more complicated, and these diagrams are no longer in the class corresponding to the kinetic equation. The next section is devoted to the analysis of these diagrams.

We note here only that in the skeleton phonon diagrams of the type of Fig. 8 each of the electron lines joining x and x' consists of lines of only one type (either single or double). Therefore the picture duplicates to a considerable degree the situation considered above as applied to impurity scattering (cf. Sec. 3). In particular, owing to the subsequent integration with respect to frequency in formula (10), it is necessary to retain in the correlators \mathcal{P}^a only the Green's-function products $G^+(\epsilon + \omega)G^-(\epsilon)$.

Let us dwell in conclusion on the physical meaning of the performed selection of the diagrams. Berezinskii has shown that in the case of scattering by impurities certain diagrams that can be omitted in the derivation of the kinetic equation in the three-dimensional situation become in the one-dimensional situation of the same order of magnitude as the diagrams taken into account in the kinetic equation. The reason lies in the multiple interference of the electrons scattered by the impurity centers. As a result, in addition to the usual criteria for the applicability of the kinetic equation, $\omega/\epsilon \ll 1$ and $\epsilon\tau_i \gg 1$, a new criterion arises, namely $\omega\tau_i \gg 1$.

The classification given by us above for the phonon diagrams has shown that the essential phonon lines are those shown in Fig. 5. They give rise to a class of phonon diagrams of the type of Fig. 8, summation of which leads to the usual kinetic equation. However, the criteria under which these diagrams dominate turned out to be quite unusual. All the discarded diagrams are of the order of $(\epsilon\tau_{ph})^{-1}$ in the three-dimensional case. In the one-dimensional case some of them acquire a value $(\bar{\omega}\tau_{ph})^{-1} = (\epsilon\tau_{ph})^{-1}/\beta$ or even $(\epsilon\tau_{ph})^{-1}/\beta^2$ (Figs. 6b–6d and Fig. 7b). At $\beta \ll 1$ these criteria differ very strongly.

We note that we are operating in an approximation in which polaron corrections to the electronic spectrum are neglected. Therefore the contribution from the diagrams of Figs. 6 and 7 is connected with interference effects in electron-phonon scattering. The anomalously large value of their contribution must be attributed to the specific character of this interference in the one-dimensional system. It is interesting that this effect is particularly strong in a degenerate gas. Indeed, the factor $(\bar{\omega}\tau_{ph}\beta)^{-1}$ is due to the rotating phonon vertices; the simplest diagram of this type is shown in Fig. 9. In these diagrams the internal vertices always give rise to additional factors of the type $n(1-n)$ and it is natural to connect them with the electron interaction via the phonons. From this point of view, the appearance of stringent limitation on the side of small $\bar{\omega}$ can be regarded as a manifestation of the "infrared" divergences

typical of one-dimensional systems.^[16,17] In the Boltzmann case ($n \rightarrow 0$) the role of the interference effect is determined entirely by the factor $(\bar{\omega}\tau)^{-1}$.

In confining ourselves to the ladder diagrams of Fig. 8, we have neglected all the interference effects brought about by the scattering of electrons by phonons. In this approximation we can trace the manner in which the localized states are gradually destroyed with increasing electron-phonon coupling (these states are due to the interference effects in the impurity scattering of the electron), and how the system goes over into the usual resistance regime determined by the electron-phonon scattering.

6. INDEPENDENCE OF THE ELECTRON BLOCKS WITH DIFFERENT ENERGIES

Our final purpose is to calculate the correlators and simultaneously take into account the interactions with the phonons and impurities. The skeleton diagram of Fig. 8 must therefore be encumbered by including all possible impurity lines.

Consider for example the diagram of Fig. 10, which contains on phonon line. This line divides the diagram into two blocks, in one of which the electron lines have energy ϵ and $\epsilon + \omega$, and in the other energy $\epsilon - \Omega$ and $\epsilon - \Omega + \omega$. We investigated first the contribution from the impurity lines joining electron lines of different blocks.

It was indicated in the preceding section that electron lines with different energies can be joined only by impurity lines that do not contain rotating vertices, i.e., by lines b, b' , and d of Fig. 3. We consider, taking these lines into account, the derivation of the equations for that part of the diagram of Fig. 10 which lies to the right of the point x ; we shall denote this part by \mathcal{R} . The equations for \mathcal{R} are derived in analogy with the derivation of Eqs. (16) for the right-hand parts in the impurity problem. Since the impurity lines with rotating vertices join only single and double electron lines with equal energy, it follows that in any section of the diagram the number of single line with given energy is equal to the number of double lines having the same energy (more accurately, differing by the small external frequency ω). We denote by m_1 the number of pairs of single

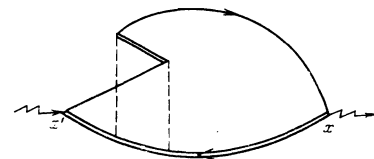


FIG. 9. Example of diagram containing the factor $n(\bar{\omega}\tau_{ph})^{-1}$.

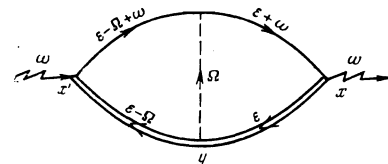


FIG. 10. Schematic representation of a diagram for the density correlator with a single phonon line. The diagram is drawn for $x' < y < x$. The impurity lines that enable the electron lines of the diagram to "crawl out" behind x and x' .

lines with energy $\epsilon + \omega$, passing through the diagram section $x + 0$. The equation for $\mathcal{R}_{m_1 m_2}$ is (see Fig. 11)

$$-\frac{d}{dx} \mathcal{R} = (\hat{V}_1 + \hat{V}_2 + \hat{V}_{12}) \mathcal{R}, \quad (44)$$

where the operators \hat{V}_1 and \hat{V}_2 correspond to inclusion of the impurity lines within the groups of electron lines with equal energy, and \hat{V}_{12} corresponds to inclusion of the impurity lines between these groups. The quantities $\hat{V}_1 \mathcal{R}$ and $\hat{V}_2 \mathcal{R}$ are constructed in analogy with (16):

$$\begin{aligned} (\hat{V}_1 \mathcal{R})_{m_1 m_2} &= \frac{m_1^2}{l_i^-(\epsilon)} \{ \mathcal{R}_{m_1-1, m_2} e^{2i\omega x/v(\epsilon)} + \mathcal{R}_{m_1+1, m_2} e^{-2i\omega x/v(\epsilon)} - 2\mathcal{R}_{m_1, m_2} \}, \\ (\hat{V}_2 \mathcal{R})_{m_1 m_2} &= \frac{m_2^2}{l_i^-(\epsilon - \Omega)} \{ \mathcal{R}_{m_1, m_2-1} e^{2i\omega x/v(\epsilon - \Omega)} + \mathcal{R}_{m_1, m_2+1} e^{-2i\omega x/v(\epsilon - \Omega)} - 2\mathcal{R}_{m_1, m_2} \}. \end{aligned} \quad (45)$$

We shall show that $\hat{V}_{12} \mathcal{R} \equiv 0$. Indeed, the electron lines with different energies are joined only by the impurity lines b (b') and d of Fig. 3. The lines b (b') correspond in this case to the factors $[-(l_i^+(\epsilon) l_i^+(\epsilon - \Omega))^{-1/2} - \Omega]^{-1/2}$, while the lines d correspond to the factors $(l_i^+(\epsilon) l_i^+(\epsilon - \Omega))^{-1/2}$. Summation over all the line therefore yields

$$\begin{aligned} (\hat{V}_{12} \mathcal{R})_{m_1 m_2} &= \{-2m_1 m_2 (l_i^+(\epsilon) l_i^+(\epsilon - \Omega))^{-1/2} \\ &\quad + 2m_1 m_2 (l_i^+(\epsilon) l_i^+(\epsilon - \Omega))^{-1/2}\} \mathcal{R}_{m_1 m_2} = 0. \end{aligned} \quad (46)$$

Turning to Eq. (44) we see that when $\hat{V}_{12} \mathcal{R} \equiv 0$ is taken into account the solution of this equation can be factorized:

$$\mathcal{R}_{m_1 m_2}(\epsilon, \epsilon - \Omega, \omega, x) = R_{m_1}(\epsilon, \omega, x) R_{m_2}(\epsilon - \Omega, \omega, x), \quad (47)$$

where $R_m(x)$ is determined from (16). This factorization shows that the diagram blocks corresponding to the lines with energies ϵ and $\epsilon - \Omega$ can be calculated independently of each other. Since the point y for the block with energy ϵ can be regarded as the position of the left-hand outer vertex (and as its right-hand vertex for the second block), we have for the diagram of Fig. 10

$$\begin{aligned} &\sum_{n_1, n_2} L_{n_1}(\epsilon - \Omega, \omega, x') Z_{n_1 n_2}(\epsilon - \Omega, \omega, x', y) R_{n_2}(\epsilon - \Omega, \omega, y) \\ &\quad \times \sum_{n_1, m_1} L_{n_1}(\epsilon, \omega, y) Z_{n_1 m_1}(\epsilon, \omega, y, x) R_{m_1}(\epsilon, \omega, x), \end{aligned} \quad (48)$$

where L are the left-hand parts. Formula (48) was written out as applied to the diagram of Fig. 10, which contains a phonon line of the type of Fig. 5b; this line corresponds to a contribution $L^+ D$. The diagrams containing phonon lines of other types correspond to expressions that differ somewhat from (48). For example,

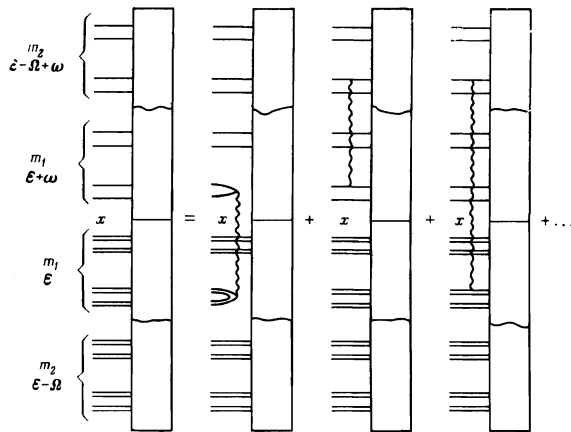


FIG. 11. Scheme for the construction of the right-hand sides. The joining of only three impurity lines is shown by way of example.

the lines Fig. 5b corresponds to the substitution $R_{n_2} \rightarrow R_{n_2+1}$ in the phonon factor $L^+ D$. This difference becomes insignificant in the important limiting case $\nu \ll 1$, to which we confine ourselves below. In this case R_n with $n \sim \nu^{-1} \gg 1$ predominate. Since $R_{n+1} = R_n(1 + O(1/n))$, we neglect the difference between R_n and R_{n+1} , the resultant error being $\sim \nu \ll 1$. As a result, in the lowest-order approximation in $\nu \ll 1$, we obtain for the diagrams of the type of Fig. 10, after summing over all types of phonon lines and external vertices,

$$\begin{aligned} &4i \int dy \int \frac{d\Omega}{2\pi} n(\epsilon - \Omega) (1 - n(\epsilon - \Omega)) \frac{L^+ + L^-}{2} ((1 - n(\epsilon)) D_{12}(\Omega) \\ &\quad + n(\epsilon) D_{21}(\Omega)) \frac{1}{v(\epsilon)} X^0(\epsilon, \omega, x - y) \frac{1}{v(\epsilon - \Omega)} X^0(\epsilon - \Omega, \omega, y - x'), \end{aligned} \quad (49)$$

where the integration with respect to y is along the entire axis. It follows therefore that in the momentum representation the diagram of Fig. 8 breaks up into a product of blocks with different electron energies, separated by phonon lines. These blocks must be calculated independently, with allowance for all the impurity lines and phonon lines a (a') of Fig. 5, with integration over all the phonon frequencies.

7. CALCULATION OF THE CONDUCTIVITY

Individual blocks with fixed electron energy differ from the electron correlators in the pure impurity problem only in the presence of self-energy inserts of the type a (a') of Fig. 5, corresponding to outflow of the particles from a given state as a result of interaction with the phonons. They can therefore be obtained in analogy with the procedure in Sec. 3. In particular, the equations for the right-hand sides \bar{R} ,

$$-\frac{d\bar{R}_m}{dx} = \frac{m^2}{l_i^-} \{ \bar{R}_{m-1} e^{2i\omega x/v} + \bar{R}_{m+1} e^{-2i\omega x/v} - 2\bar{R}_m \} - \frac{2m}{v\tau_{ph}} \bar{R}_m, \quad (50)$$

differ from (16) only in the last term. The time of relaxation on the phonons, which enters in this term, is given by

$$\begin{aligned} \frac{1}{\tau_{ph}(\epsilon)} &= i \int \frac{d\Omega}{2\pi} \frac{1}{2v(\epsilon - \Omega)} [L^+ + iL_+^0 + L^- - iL_-^0 + L^+ - iL_+^0 + L^- + iL_-^0] \\ &\quad \times [(1 - n(\epsilon - \Omega)) D_{21}(\Omega) + n(\epsilon - \Omega) D_{12}(\Omega)] = \int d\epsilon' W(\epsilon', \epsilon), \end{aligned} \quad (51)$$

where

$$\begin{aligned} W(\epsilon', \epsilon) &= W^+(\epsilon', \epsilon) + W^-(\epsilon', \epsilon), \\ W^\pm(\epsilon', \epsilon) &= \int \frac{d^3q}{(2\pi)^3} |c_q|^2 \frac{1 - n(\epsilon')}{1 - n(\epsilon)} \frac{1}{v(\epsilon')} \delta(q_x + p(\epsilon) \mp p(\epsilon')) \\ &\quad \times [(N_q + 1) \delta(\epsilon - \epsilon' - \omega_q) + N_q \delta(\epsilon - \epsilon' + \omega_q)]. \end{aligned} \quad (52)$$

The terms iL_\pm^0 cancel out when the contributions from the single and double lines are summed (in perfect analogy with (18)).

The quantity $W(\epsilon', \epsilon)$ is the probability of the outflow from the state ϵ into the state ϵ' ; it enters in the linearized kinetic equation and satisfies therefore the relation

$$v(\epsilon') n(\epsilon) (1 - n(\epsilon)) W(\epsilon', \epsilon) = v(\epsilon) n(\epsilon') (1 - n(\epsilon')) W(\epsilon, \epsilon'). \quad (53)$$

If we use the substitution $\bar{R}_m(x) = \bar{R}_m e^{2im\omega x/v}$ to change over to equations of the type (23), then we see that

$$\bar{R}_m(\omega) = R_m(\omega + i/\tau_{ph}). \quad (54)$$

The central and left parts \bar{Z} and \bar{L} are perfectly analogously expressed in terms of Z and L . As a result, the contributions of the individual blocks are obtained from the corresponding correlators for the pure impurity problem by a frequency shift equal to i/τ_{ph} .

The criterion $|\nu| \ll 1$ used above both in the derivation of (49) and in the determination of the explicit form of the electron correlators for the impurity potential (see Sec. 4) reduces, when the frequency shift is taken into account, to a simultaneous satisfaction of the conditions

$$\omega\tau_i \ll 1, \quad \tau_i/\tau_{ph} \ll 1. \quad (55)$$

The second of these conditions denote weakness of the scattering by phonons in comparison with the impurity scattering.

The diagram expansions of the type of Fig. 8 for the current-current correlators \mathcal{F}^1 contain current operators in the external vertices x and x' . All the internal blocks (e.g., between the points y_1 and y_2 of Fig. 8) are equivalent to the density-density correlators of the impurity problem. The two outer blocks (between y_1 and x and between y_2 and x') are equivalent to the current-density correlators of the impurity problem. Calculation of these latter correlators shows that they are proportional to the quantities $Q_m(\kappa) - Q_m(-\kappa)$, which vanish as $\kappa \rightarrow 0$. Therefore, as $\kappa \rightarrow 0$, from among all the ladder diagrams of the type of Fig. 8 we are left only with the simplest ones consisting of one block. It constitutes the current-current correlator for the impurity problem with shifted frequency. Therefore, taking (10) and (19) into account, we have

$$\mathcal{X}^1(\epsilon, \omega) = X^1(\epsilon, \omega + i/\tau_{ph}). \quad (56)$$

The final formula for the conductivity follows from this with allowance for (4), (19), and (38)

$$\sigma(\omega) = \frac{8}{\pi} \zeta(3) e^2 \int \frac{d\epsilon}{v(\epsilon)} \left(-\frac{\partial n}{\partial \epsilon} \right) (l_i^-(\epsilon))^2 \left(-i\omega + \frac{1}{\tau_{ph}(\epsilon)} \right). \quad (57)$$

It becomes simpler for a strongly degenerate gas:

$$\sigma(0) = \frac{8}{\pi} \zeta(3) e^2 v_F \tau_i^2 \tau_{ph}^{-1}, \quad (58)$$

v_F is the Fermi velocity. If we compare (57) with the usual formula that follows from the kinetic equation, then we obtain for the effective free path and for the effective free-path time

$$l(\epsilon) = v(\epsilon) \tau(\epsilon) = 4\zeta(3) l_i^-(\epsilon) \tau_i(\epsilon) / \tau_{ph}(\epsilon). \quad (59)$$

According to (58), the conductivity is due entirely to the electron-phonon interaction and increases in direct proportion to the rate of electron scattering by the phonons. We see that both types of phonon scattering, with momentum transfers $|\Delta p| \approx 2p_F$ and $|\Delta p| \ll p_F$ enter perfectly symmetrically in formula (51) for τ_{ph} . This means that the delocalization of the electrons occurs when they are scattered by the phonons both forward and backward. At low temperatures $T < \omega_D$, the first type of scattering dominates.

At $\tau_{ph} \gg \tau_i$ the effective time is $\tau \sim \tau_i^2 / \tau_{ph} \ll \tau_i$. The temperature dependence of τ_{ph} is determined by the ratio of a number of parameters. For a one dimensional metal we have $\tau_{ph}^{-1} \propto T^3$ and $\tau_{ph}^{-1} \propto T$ at $T \ll \omega_D$ and $T \gtrsim \omega_D$, respectively (ω_D is the Debye frequency). Therefore τ , and consequently also σ , first increases like T^3 and then like T . At the boundary of the region of applicability of (57) we have $\tau_{ph} \sim \tau_i$ and the time τ reaches a value $\tau \sim \tau_i$.

8. ELECTRON DIFFUSION

It was shown in the preceding section that the static conductivity of the electron system assumes a finite

value if account is taken, besides the electron-impurity interaction, also of the weak electron-phonon interaction. It must be assumed that the finite value of the conductivity is due to delocalization of the electronic states as a result of the interaction of the electrons with the phonons. We shall calculate the density correlator with an aim at following the diffusion of the electrons under these conditions.

The diagram series for the density correlator is a ladder of the type shown in Fig. 8, each block of which is an electron-density correlator in an impurity field with shifted frequency (see (54)) and is equal to $X^0(\epsilon, \omega + i/\tau_{ph}, k)$. It is convenient to sum this series by writing down the equation for the quantity $\mathcal{X}^0(\epsilon, \omega, k)$, which is connected with the density correlator by the relation

$$\mathcal{X}^0(\omega, k) = 2 \int \frac{d\epsilon}{2\pi} \mathcal{X}^0(\epsilon, \omega, k). \quad (60)$$

The actual form of the equation can be easily established by recognizing that its first iteration is given by (49). As a result we get

$$\begin{aligned} \mathcal{X}^0(\epsilon, \omega, k) = & n(\epsilon) (1-n(\epsilon)) \frac{2}{v(\epsilon)} X^0\left(\epsilon, \omega + \frac{i}{\tau_{ph}}, k\right) \\ & + \frac{2}{v(\epsilon)} X^0\left(\epsilon, \omega + \frac{i}{\tau_{ph}}, k\right) i \\ & \times \int \frac{d\Omega}{2\pi} \frac{L^+ + L^-}{2} [(1-n(\epsilon)) D_{12}(\Omega) + n(\epsilon) D_{21}(\Omega)] \mathcal{X}^0(\epsilon - \Omega, \omega, k). \end{aligned} \quad (61)$$

Taking into account the explicit form of $X^0(\epsilon, \omega, k)$ at $|\nu| \ll 1$ and $|\kappa| \gg 1$ (see (34)), we obtain in the coordinate-time representation and at $|x| \gg l_1^-$ and $t \gg \tau_i$ the following equation:

$$\begin{aligned} \frac{\partial}{\partial t} \mathcal{X}^0(\epsilon, t, x) = & 4\zeta(3) (l_i^-(\epsilon))^2 \int d\epsilon' W(\epsilon, \epsilon') \frac{\partial^2}{\partial x^2} \mathcal{X}^0(\epsilon', t, x) \\ & + \int d\epsilon' [W(\epsilon, \epsilon') \mathcal{X}^0(\epsilon', t, x) - W(\epsilon', \epsilon) \mathcal{X}^0(\epsilon, t, x)]. \end{aligned} \quad (62)$$

This equation lends itself to a simple interpretation. The first term in the right-hand side describes the phonon-induced spatial diffusion of the electron, wherein electron hops take place at time intervals $\sim \tau_{ph}$ over a distance $\sim l_1^-$ that determines the dimension of the region of the electron localization in the impurity field. The second term coincides with the linearized collision integral and determines the energy relaxation of the electrons in a given point of space.

We shall show that at long times $t \gg \tau_{ph}$ and in the case of weak spatial inhomogeneity the density correlator $\mathcal{X}^0(t, x)$ satisfies the diffusion equation. To this end we integrate (62) with respect to ϵ . The integral of the second term in the right-hand side vanishes identically for all functions $\mathcal{X}^0(\epsilon, t, x)$. In the resultant equation

$$\frac{\partial}{\partial t} \mathcal{X}^0(t, x) = 4\zeta(3) \int \frac{d\epsilon}{\pi} (l_i^-(\epsilon))^2 \int d\epsilon' W(\epsilon, \epsilon') \frac{\partial^2}{\partial x^2} \mathcal{X}^0(\epsilon', t, x) \quad (63)$$

it is necessary to substitute $\mathcal{X}^0(\epsilon', t, x)$ in the form

$$\mathcal{X}^0(\epsilon', t, x) = \frac{1}{v(\epsilon')} n(\epsilon') (1-n(\epsilon')) N(t, x), \quad \int dx N(t, x) = 1, \quad (64)$$

since it is just this expression that causes the vanishing of the collision integral, which is literally the principal term in (62). We then obtain for the function $N(t, x)$ the diffusion equation

$$\frac{\partial}{\partial t} N(t, x) = D \frac{\partial^2}{\partial x^2} N(t, x). \quad (65)$$

The diffusion coefficient

$$D=4\zeta(3) \int \frac{d\epsilon}{v(\epsilon)} \frac{\partial n}{\partial \epsilon} (l_i^-(\epsilon))^2 \frac{1}{\tau_{ph}(\epsilon)} \bigg/ \int \frac{d\epsilon}{v(\epsilon)} \frac{\partial n}{\partial \epsilon} \quad (66)$$

is connected with the mobility u by the Einstein relation

$$D=u \int \frac{d\epsilon}{v(\epsilon)} n(\epsilon) \bigg/ \int \frac{d\epsilon}{v(\epsilon)} \left(-\frac{\partial n}{\partial \epsilon}\right), \quad (67)$$

which follows from (66) and (57).

If the criterion $\bar{\omega}/T \ll 1$ is satisfied and the spatial gradients are large enough to have $l_i^- \partial \bar{\mathcal{E}}^0 / \partial x \gg \bar{\omega} \mathcal{E}^0 / T$, then the spatial diffusion takes place independently at each energy level in accord with the equation

$$\frac{\partial}{\partial t} \mathcal{E}^0(\epsilon, t, x) = 4\zeta(3) \frac{(l_i^-(\epsilon))^2}{\tau_{ph}(\epsilon)} \frac{\partial^2}{\partial x^2} \mathcal{E}^0(\epsilon, t, x), \quad (68)$$

where $4\zeta(3) (l_i^-(\epsilon))^2 / \tau_{ph}(\epsilon) = D(\epsilon)$ is the diffusion coefficient of an electron with energy ϵ .

CONCLUSION

Let us summarize our results.

The decrease of the wave functions of the electrons in an impurity field is characterized by the asymptotic behavior of the density correlator at large distances and long times

$$\rho_{\infty}(x) \propto |x|^{-2} \exp(-|x|/4l_i^-).$$

Here $l_i^-(\epsilon)$ is the mean free path of an electron of energy ϵ in the impurity field; this length is calculated in the usual manner from its backscattering amplitude. The presence of a power-law factor alongside with the exponential is due to the fact that the asymptotic form is determined not by a pole but by a branch point in k -plane.

The conductivity and the diffusion coefficient are determined by formulas (57) and (66). They correspond fully to picture in which the electron moves by diffusion but executes hops over a distance $\sim l_i^-(\epsilon)$ with a frequency $\tau_{ph}^{-1}(\epsilon)$ corresponding to the reciprocal electron-phonon scattering time. The quantity τ_{ph}^{-1} includes two contributions, from scattering with small ($\Delta p \ll p_F$) and with large ($\Delta p \approx 2p_F$) momentum transfers (p_F is the Fermi momentum). At low temperatures, the first contribution predominates; at high temperatures they are of the same order. The temperature dependence of the conductivity should be of the type $\sigma \propto T^3$ or $\sigma \propto T$, depending on the ratio of T to the phonon Debye frequency.

Of course, a regime in which scattering by phonons induces conductivity is possible only if $\tau_{ph} \gtrsim \tau_i = l_i^- / v_F$. In the opposite limiting case the scattering by the phonons is the main mechanism of the resistivity, and the conductivity can be determined from the kinetic equation

$$\sigma(0) = \frac{2}{\pi} e^2 \int d\epsilon v(\epsilon) \left(-\frac{\partial n}{\partial \epsilon}\right) \tau_{ph}(\epsilon). \quad (69)$$

Here, as usual, σ is proportional to the relaxation time. It is important that (69), in contrast to (57), contains only phonon backscattering (i.e., with a transfer $\Delta p \approx 2p_F$).

From a comparison of (57) and (69) it follows that for quasi-one-dimensional metals the temperature dependence of σ should have a maximum (corresponding to $\tau_{ph} \sim \tau_i$) and the temperature dependence should be of the type shown in Fig. 12. Similar dependences were

indeed observed for certain systems,^[18] but their origin is not yet clear.

In the derivation of the fundamental equations it was necessary to assume, besides the usual condition $\epsilon T \gg 1$, also that $\bar{\omega} \tau_i, \bar{\omega} \tau_{ph} \gg 1$ and $\bar{\omega} \tau_{ph} \bar{\omega} / \epsilon \gg 1$. At $\bar{\omega} \ll \epsilon$ these criteria are much more stringent than the first one. The criteria containing τ_{ph} are the condition for the suppression of the interference effects in phonon scattering, which has turned out to be very strong in the one-dimensional system. It appears that they are of the same character as the interference effects that lead to localization in impurity scattering. It is interesting that the last and most stringent criterion drops out for non-degenerate electrons.

We did not take into account electron interaction, whether direct or via phonons. The latter is formally small because of the electron-phonon coupling constant and can be left out if it does not lead to a restructuring of the spectrum, as is indeed assumed.

We calculated above the conductivity in a homogeneous electric field and did not consider the usual effects of the percolation type.^[19] If $T \tau_i \gg 1$, then a section of length l_i^- in a layer of thickness T will contain many levels, and the fluctuations will be small on the average. Flow around the sections with large resistance will be due to the finite conductivity between the filaments and the displacement currents (at $\omega \neq 0$), and the conductivity is then given by (57).

We are grateful to V. L. Berezinskiĭ, L. P. Gor'kov, and G. M. Eliashberg for a discussion of the results.

APPENDIX

In the main text we have considered diagrams of the electron-loop type of Fig. 1; we shall now indicate the reason why more complicated diagrams can be omitted, with the density correlator as example.

The diagrams of type a in Fig. 13, in which the electron loops are connected by an impurity line, vanish identically at $\omega \neq 0$. The phonon line joining the loops

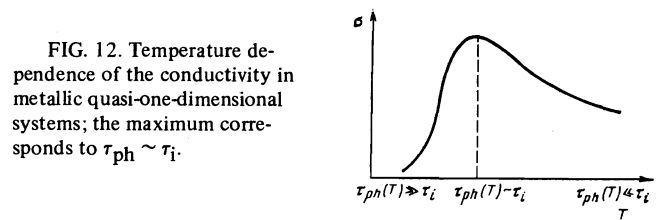


FIG. 12. Temperature dependence of the conductivity in metallic quasi-one-dimensional systems; the maximum corresponds to $\tau_{ph} \sim \tau_i$.

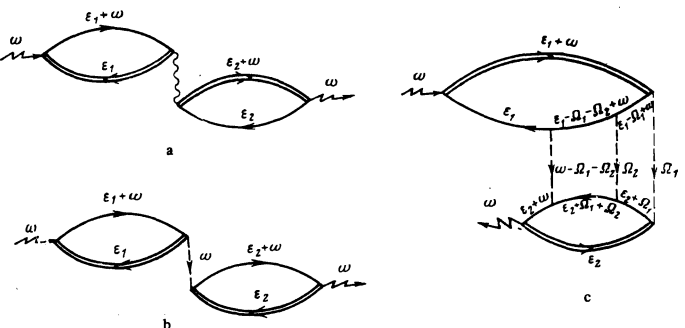


FIG. 13. Correlator diagrams that include several electron loops.

on Fig. 13b corresponds to a factor of the type

$$(D_{11}(\omega) - D_{12}(\omega)) (n(\varepsilon_2) - n(\varepsilon_2 + \omega)).$$

It is of the order of $\omega/T\tau_{ph}$ and the individual loops, in analogy with (34), are of the order of ω^{-1} . Therefore the diagrams b of Fig. 13 are small in comparison with Fig. 1 if $(T\tau_{ph})^{-1} \ll 1$. Since $\bar{\omega} \lesssim T$, this criterion is here not stronger than $(\bar{\omega}\tau_{ph})^{-1} \ll 1$, which was used in Sec. 5. In diagrams of type c of Fig. 13, in contrast to diagram b, the frequency corresponding to the phonons is not small. But in these diagrams the phonon lines join electron lines with different energies, so that the diagrams are small because of the parameter $(\bar{\omega}\tau_{ph}\beta)^{-1} \ll 1$ (cf. Sec. 5).

Since each of the loops is proportional to the electron occupation numbers n , it follows that for a non-degenerate gas all the diagrams of Fig. 13 are small because of the parameter $n \ll 1$.

¹⁾The value $A = 2(\pi^2 - C_3)$ given in [11] for this integral is in error.

¹F. J. Dyson, Phys. Rev., **92**, 1331 (1953). M. Lax and J. C. Phillips, Phys. Rev., **110**, 41 (1958). H. L. Frisch and S. R. Lloyd, Phys. Rev., **120**, 1175 (1960). B. I. Halperin, Phys. Rev., **139**, A 104, (1965); Adv. Chem. Phys., **13**, 123 (1967). J. Hori, Progr. Theor. Phys., **31**, 940 (1964); Suppl., **36**, 3 (1967).

²I. F. Shchegolev, Phys. Stat. Sol. (a), **12**, 9 (1972).

³N. F. Mott and W. D. Twose, Adv. Phys., **10**, 107 (1961).

⁴R. E. Borland, Proc. Phys. Soc., **78**, 926 (1961); **A274**, 529 (1963).

⁵E. N. Economou and M. H. Cohen, Phys. Rev., **4**, B396 (1971). C. T. Papatrifiantillou, Phys. Rev. **7**, B5386 (1973).

⁶P. W. Anderson, Phys. Rev., **109**, 1492 (1958).

⁷I. M. Lifshitz, Usp. Fiz. Nauk **83**, 617 (1964) [Sov. Phys.-Uspekhi **7**, 549 (1965)].

⁸V. L. Bonch-Bruevich, Zh. Eksp. Teor. Fiz. **61**, 1168 (1971) [Sov. Phys.-JETP **34**, 623 (1971)].

⁹R. Abou-Chacra, P. W. Anderson, and D. J. Thouless, J. Phys. C: Solid State Phys., **6**, 1734 (1973).

¹⁰Yu. A. Bychkov, Zh. Eksp. Teor. Fiz. **65**, 427 (1973) [Sov. Phys.-JETP **38**, 209 (1974)].

¹¹V. L. Berezinskiĭ, Zh. Eksp. Teor. Fiz. **65**, 1251 (1973) [Sov. Phys.-JETP **38**, 620 (1974)].

¹²N. F. Mott, Phil. Mag., **19**, 835 (1969).

¹³L. V. Keldysh, Zh. Eksp. Teor. Fiz. **47**, 1515 (1964) [Sov. Phys.-JETP **20**, 1018 (1965)].

¹⁴G. M. Eliashberg, Zh. Eksp. Teor. Fiz. **41**, 1241 (1961) [Sov. Phys.-JETP **14**, 886 (1962)].

¹⁵I. S. Gradshteĭn and I. M. Ryzhik, Tablitsy intergalov (Tables of Integrals), Nauka (1971).

¹⁶Yu. A. Bychkov, L. P. Gor'kov, and I. E. Dzyaloshinskiĭ, Zh. Eksp. Teor. Fiz. **50**, 738 (1966) [Sov. Phys.-JETP **23**, 489 (1966)].

¹⁷A. Luther and I. Peschel, Phys. Rev., **9**, B2911 (1974).

¹⁸L. I. Buravov, D. N. Sedutin, and I. F. Shchegolev, Zh. Eksp. Teor. Fiz. **59**, 1125 (1970) [Sov. Phys.-JETP **32**, 612 (1971)]; M. I. Cohen, L. V. Coleman, A. F. Garito, and A. I. Heeger, Phys. Rev. **B10**, 1298 (1974).

¹⁹B. I. Shkolvskii, Fiz. Tekh. Poluprovodn. **6**, 1197 (1972) [Sov. Phys.-Semicond. **6**, 1053 (1973)].

Translated by J. G. Adashko

35